



**HAL**  
open science

## Bubble physics

Michiel Postema

► **To cite this version:**

Michiel Postema. Bubble physics. Michiel Postema. Fundamentals of Medical Ultrasonics, Spon Press, pp.177-204, 2011, 978-0-415-56353-6. 10.5281/zenodo.4777637 . hal-03198001

**HAL Id: hal-03198001**

**<https://hal.science/hal-03198001>**

Submitted on 1 May 2021

**HAL** is a multi-disciplinary open access archive for the deposit and dissemination of scientific research documents, whether they are published or not. The documents may come from teaching and research institutions in France or abroad, or from public or private research centers.

L'archive ouverte pluridisciplinaire **HAL**, est destinée au dépôt et à la diffusion de documents scientifiques de niveau recherche, publiés ou non, émanant des établissements d'enseignement et de recherche français ou étrangers, des laboratoires publics ou privés.

# Chapter 8: Bubble physics

Michiel Postema

Postema M. Bubble physics. In: Postema M. Fundamentals of Medical Ultrasonics. London: Spon Press, pp. 177–204, 2011, ISBN 978-0-415-56353-6.

This is an Accepted Manuscript of a book chapter published by Routledge/CRC Press in Fundamentals of Medical Ultrasonics on February 23, 2011, available online:

<https://www.routledge.com/9780415563536>

<https://www.crcpress.com/9780415563536>

<https://dx.doi.org/10.1201/9781482266641>



# Chapter 8

## Bubble physics

The density and compressibility parameters of blood cells hardly differ from those of plasma. Therefore, blood cells are poor scatterers in the clinical diagnostic frequency range. Since imaging blood flow and measuring organ perfusion are desirable for diagnostic purposes, markers should be added to the blood to differentiate between blood and other tissue types. Such markers must be acoustically active in the medical ultrasonic frequency range.

Figure 8.1 shows the resonance frequencies of free and encapsulated gas microbubbles as a function of their equilibrium radius. The resonance frequencies of encapsulated microbubbles lie slightly higher than those of free gas bubbles, but clearly well within the clinical diagnostic range, too. Based on their acoustic properties, microbubbles are well suited as an ultrasound contrast agent.

In this chapter, microbubble behaviour in an ultrasound field is explored, with special attention to the influence of the bubble shell.

### 8.1 Hollow sphere

Consider a thin-shelled sphere in equilibrium. Assume  $p_s$  to be the difference between the internal pressure and the ambient pressure, generally referred to as the surface pressure. For any cross-sectional area  $A$  through the centre of the sphere, the following force balance must hold:

$$p_s A = \sigma S, \quad (8.1)$$

where  $S$  is the path around the area and  $\sigma$  is the surface tension. Introducing the radius  $R$  yields

$$p_s (\pi R^2) = \sigma (2\pi R), \quad (8.2)$$

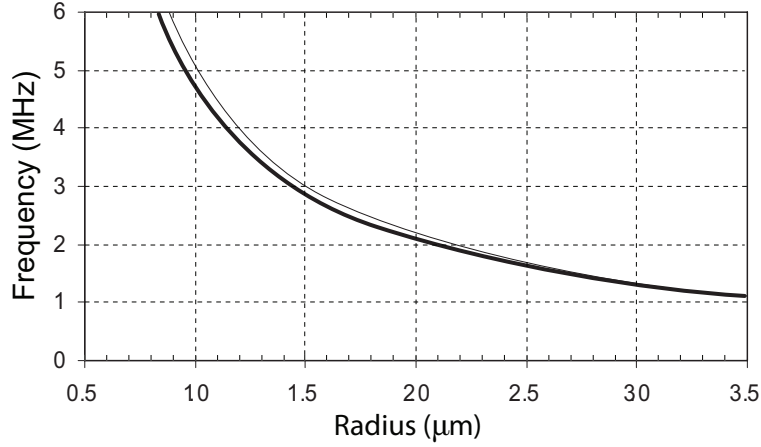


Figure 8.1: Resonance frequencies of free (bold line) and lipid-encapsulated (thin line) air microbubbles in water as a function of equilibrium radius.

which equates to

$$p_s = \frac{2\sigma}{R}. \quad (8.3)$$

Hence, the smaller the bubble, the higher the difference between the internal pressure and the ambient pressure. Since fluids are forced to flow from a location with a higher pressure to a location with a lower pressure, a bubble without an impenetrable solid shell cannot exist in true equilibrium.

## 8.2 Cavitation threshold

Now, consider a polytropic gas bubble in an infinite liquid. The following unstable equilibrium can be formulated:

$$p_g + p_v = p_0 + \frac{2\sigma}{R_0}, \quad (8.4)$$

where  $p_g$  is the gas pressure,  $p_v$  is the vapour pressure,  $p_0$  is the ambient pressure, and  $R_0$  is the quasi-equilibrium radius of the bubble.

If buoyancy and gas diffusion are slow compared with a change in ambient pressure,

$$p_g V^\gamma = \text{constant}, \quad (8.5)$$

where  $V$  is the bubble volume and  $\gamma$  is the ratio of specific heats of the gas. For air,  $\gamma = 1.4$  is a good approximation. Substituting (8.4) for the gas

pressure gives for any situation  $n$

$$\left(p_0 - p_v + \frac{2\sigma}{R_0}\right) V_0^\gamma = p_n V_n^\gamma, \quad (8.6)$$

where  $V_0$  is the quasi-equilibrium bubble volume. Changing the liquid pressure instantaneously, so that the liquid pressure at the bubble wall is  $p_L$ , gives

$$\left(p_0 - p_v + \frac{2\sigma}{R_0}\right) V_0^\gamma = \left(p_L - p_v + \frac{2\sigma}{R}\right) V^\gamma. \quad (8.7)$$

For a perfectly spherical bubble,

$$\left(p_0 - p_v + \frac{2\sigma}{R_0}\right) \left(\frac{4}{3}\pi R_0^3\right)^\gamma = \left(p_L - p_v + \frac{2\sigma}{R}\right) \left(\frac{4}{3}\pi R^3\right)^\gamma, \quad (8.8)$$

which can be rewritten as

$$p_L = \left(p_0 - p_v + \frac{2\sigma}{R_0}\right) \left(\frac{R_0}{R}\right)^{3\gamma} + p_v - \frac{2\sigma}{R}. \quad (8.9)$$

If the sonicating frequency is much lower than the bubble resonance frequency, the pressure in the liquid changes very slowly and uniformly compared with the natural time scale of the microbubble. The radius of a bubble  $R$  in response to quasistatic changes in the liquid pressure is described by (8.9). Figure 8.2 shows the right-hand side of (8.9), for different  $R_0$ .

For each curve, there exists a minimum  $(p_{cr}, R_{cr})$ , where  $R_{cr}$  is the critical radius and  $p_{cr}$  is the critical quasi-isostatic pressure. The region to the right-hand side of the critical radius represents unstable equilibrium conditions. If the liquid pressure is lowered until it reaches a value below  $p_{cr}$ , no equilibrium radius exists, resulting in explosive growth of the bubble, much larger than  $R_0$ , hence the term cavitation threshold. The ambient pressure eventually increases again, during the ultrasonic compression phase, causing the bubble to collapse violently.

The critical radius is computed, knowing that, in  $(R_{cr}, p_{cr})$ ,

$$\frac{\partial p_L}{\partial R} = 0. \quad (8.10)$$

Substituting the right-hand side of (8.9) for  $p_L$  gives

$$-3\gamma \left(p_0 - p_v + \frac{2\sigma}{R_0}\right) \frac{R_0^{3\gamma}}{R_{cr}^{3\gamma+1}} + \frac{2\sigma}{R_{cr}^2} = 0, \quad (8.11)$$

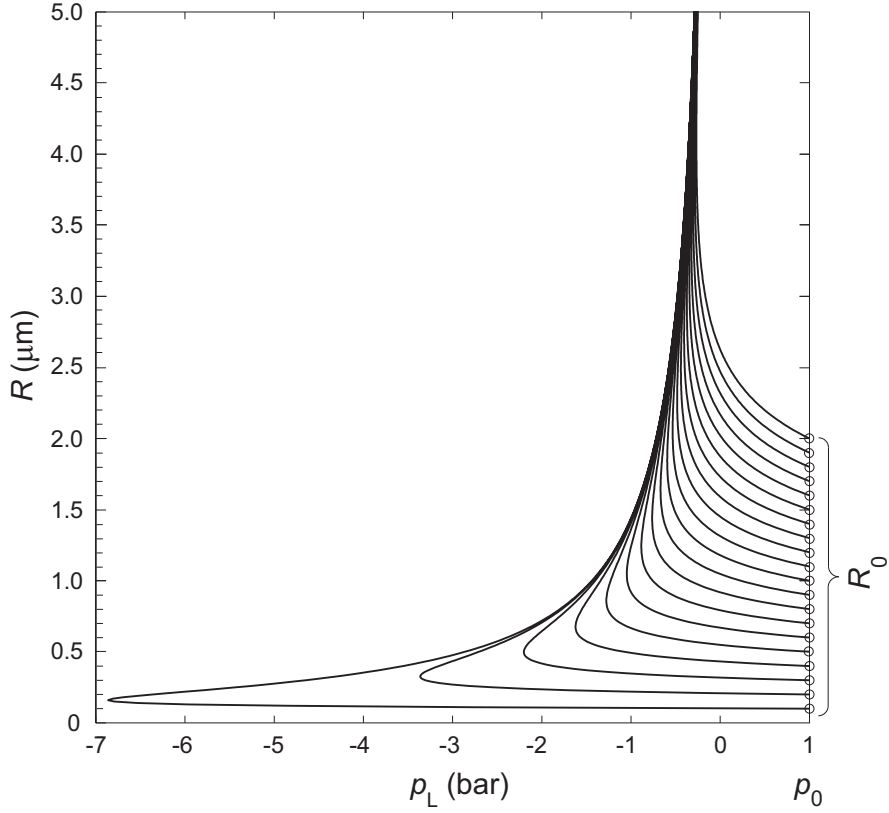


Figure 8.2: Solutions of (8.9) for different equilibrium radii  $0.1 \leq R_0 \leq 2.0 \mu\text{m}$ , taking  $p_0 = 1 \text{ atm}$ ,  $\gamma = 1.4$ , and  $\sigma = 0.072 \text{ kg s}^{-2}$ .

which equates to

$$R_{\text{cr}} = \left[ \frac{3\gamma}{2\sigma} \left( p_0 - p_v + \frac{2\sigma}{R_0} \right) R_0^{3\gamma} \right]^{\frac{1}{3\gamma-1}}, \quad (8.12)$$

from which the critical pressure follows:

$$p_{\text{cr}} = -p_0 + p_v - \frac{(6-2\gamma)\sigma}{3\gamma R_{\text{cr}}}, \quad (8.13)$$

or, as a function of  $R_0$ ,

$$p_{\text{cr}} = -p_0 + p_v - \frac{(6-2\gamma)\sigma}{3\gamma} \left[ \frac{2\sigma}{3\gamma \left( p_0 - p_v + \frac{2\sigma}{R_0} \right)} \right]^{3\gamma-1}. \quad (8.14)$$

If the situation is isothermal and if vapour pressure can be neglected, for bubbles of radius  $R_0 \ll \frac{2\sigma}{p_0}$ ,

$$p_{\text{cr}} \approx -p_0 - 0.77 \frac{\sigma}{R_0}. \quad (8.15)$$

The critical radius, also referred to as the Blake radius, has been approximated by

$$R_{\text{cr}} \approx 2R_0. \quad (8.16)$$

During the initial part of the collapse the acceleration  $\ddot{R}$  is negative. This sign changes as the gas inside the bubble begins to be compressed, and the rebound begins.

### 8.3 Fundamental equation of bubble dynamics

Consider an empty cavity with initial radius  $R_0$  that expands or contracts to  $R$ , owing to a difference between the pressure in the liquid at the bubble wall and the pressure in the liquid at infinity  $p_L - p_0^\infty$ . Here, we take  $p_0^\infty = p_0$ . In time  $\Delta t$ , the liquid mass flowing across a surface outside the bubble with radius  $r$  must equal the mass displaced by the expanding or contracting bubbles surface, *i.e.*,

$$4\pi r^2 \rho \dot{r} \Delta t = 4\pi R^2 \rho \dot{R} \Delta t. \quad (8.17)$$

Hence, the particle velocity in the liquid can be expressed in terms of  $r$ ,  $R$ , and  $\dot{R}$ :

$$\dot{r} = \frac{R^2 \dot{R}}{r^2}. \quad (8.18)$$

The work done by an expanding or contracting bubble must equal the kinetic energy of the surrounding liquid:

$$\int_{R_0}^R (p_L - p_0) 4\pi R^2 dR = \frac{1}{2} \int_R^\infty \dot{r}^2 \rho 4\pi r^2 dr. \quad (8.19)$$

Substituting (8.18) for  $\dot{r}$  simplifies the kinetic energy of the liquid to

$$E_k = 2\rho \int_R^\infty \frac{R^4 \dot{R}^2}{r^2} dr = 2\pi \rho R^3 \dot{R}^2. \quad (8.20)$$

Now the following equality should be noted:

$$\frac{\partial}{\partial R} \left( \dot{R}^2 \right) = \frac{1}{\dot{R}} \frac{\partial \dot{R}^2}{\partial t} = 2\ddot{R}, \quad (8.21)$$

so that (8.19) can be differentiated to  $R$ . This results in the fundamental equation of bubble dynamics:

$$\frac{p_L - p_0}{\rho} = R\ddot{R} + \frac{3}{2}\dot{R}^2. \quad (8.22)$$

If a bubble is subjected to a driving function  $P(t)$ , (8.22) changes to

$$\frac{p_L - p_0 - P(t)}{\rho} = R\ddot{R} + \frac{3}{2}\dot{R}^2. \quad (8.23)$$

For a polytropic gas bubble, (8.9) is substituted for  $p_L$ :

$$R\ddot{R} + \frac{3}{2}\dot{R}^2 = \frac{1}{\rho} \left[ \left( p_0 - p_v + \frac{2\sigma}{R_0} \right) \left( \frac{R_0}{R} \right)^{3\gamma} + p_v - \frac{2\sigma}{R} - p_0 - P(t) \right]. \quad (8.24)$$

## 8.4 Pressure radiated by a bubble

To compute the acoustic pressure radiated by a bubble at any point in the liquid, consider the equation of motion (4.7):

$$\frac{1}{\rho} \frac{\partial p}{\partial r} = -\frac{\partial \dot{r}}{\partial t} - \dot{r} \frac{\partial \dot{r}}{\partial r}. \quad (8.25)$$

Integrating over  $r$  gives

$$\int_r^\infty \frac{1}{\rho} \frac{\partial p}{\partial r} dr = -\int_r^\infty \frac{\partial \dot{r}}{\partial t} dr - \int_r^\infty \dot{r} \frac{\partial \dot{r}}{\partial r} dr, \quad (8.26)$$

which can be solved by substituting (8.18) for  $\dot{r}$ :

$$\frac{p(r, t) - p_0}{\rho} = -\frac{\partial}{\partial t} \left( \frac{R^2 \dot{R}}{r} \right) - \frac{1}{2} \frac{R^4 \dot{R}^2}{r^4}. \quad (8.27)$$

This is actually a representation of Bernoulli's theorem,

$$\frac{p(r, t) - p_0^\infty}{\rho} = -\frac{\partial \Phi}{\partial t} - \frac{1}{2} v^2, \quad (8.28)$$

where  $v$  is the particle velocity and  $\Phi$  is the velocity potential

$$\Phi = - \int_r^\infty \dot{r} dr. \quad (8.29)$$

The equation of motion in the liquid (8.27) can be further simplified to

$$\frac{p(r, t) - p_0}{\rho} = - \frac{2R\dot{R}^2 + R^2\ddot{R}}{r} - \frac{1}{2} \frac{R^4 \dot{R}^2}{r^4}. \quad (8.30)$$

In the far field, at distances  $r \gg R$ ,

$$\frac{p(r, t) - p_0}{\rho} = - \frac{2R\dot{R}^2 + R^2\ddot{R}}{r}. \quad (8.31)$$

## 8.5 Viscous fluids

The viscosity  $\eta$  of a Newtonian viscous fluid is by definition the ratio of stress and rate of strain  $\dot{\epsilon}$ . In viscous fluids, the relations (2.61) and (2.74) do not apply. It should be noted that the principal stresses have been defined as positive for expanding media, as opposed to the definitions in fluid physics and acoustics. If we take a hydrostatic stress  $p$ , for an incompressible liquid,

$$p_L = -p - 2\eta\dot{\epsilon}_r, \quad (8.32)$$

where  $\dot{\epsilon}_r$  is the radial rate of strain. Using (8.18), the radial rate of strain can be expressed in terms of  $r$  and  $R$ :

$$\dot{\epsilon}_r = \frac{\partial \dot{r}}{\partial r} = \frac{\partial}{\partial r} \left( \frac{R^2 \dot{R}}{r^2} \right) = - \frac{2R^2 \dot{R}}{r^3}, \quad (8.33)$$

which at the bubble surface ( $r = R$ ) becomes

$$\dot{\epsilon}_r = - \frac{2\dot{R}}{R}, \quad (8.34)$$

Combining (8.22), (8.32), and (8.34) results in

$$\frac{1}{\rho} \left( p_L - p_0 - \frac{4\eta\dot{R}}{R} \right) = R\ddot{R} + \frac{3}{2}\dot{R}^2. \quad (8.35)$$

Introducing a driving function  $P(t)$  gives an equation similar to (8.24) for a polytropic gas bubble:

$$R\ddot{R} + \frac{3}{2}\dot{R}^2 = \frac{1}{\rho} \left[ \left( p_0 - p_v + \frac{2\sigma}{R_0} \right) \left( \frac{R_0}{R} \right)^{3\gamma} + p_v - \frac{2\sigma}{R} - \frac{4\eta\dot{R}}{R} - p_0 - P(t) \right]. \quad (8.36)$$

This is the Rayleigh–Plesset equation. Note that the Rayleigh–Plesset equation can only be applied if the liquid is incompressible and if the gas is polytropic.

Figure 8.3 shows radius–time curves of two microbubbles subjected to continuous sine pressure waves with low, moderate, and high amplitudes. Both bubbles oscillate linearly at  $MI = 0.01$ . With increasing driving amplitude, asymmetries in radial excursion and expansion time rise, especially for the bigger bubble, which is closer to the resonance size. At  $MI = 0.8$ , both bubbles expand to a factor of the initial size, followed by a rapid collapse for the smaller bubble. The bigger bubble demonstrates collapses at  $MI = 0.18$  and higher.

## 8.6 Oscillations

The Rayleigh–Plesset equation describes highly nonlinear radially symmetric bubble oscillations, but at low acoustic driving amplitudes, the behaviour is linear. At such low amplitudes, a bubble behaves like a mass–spring–dashpot system and (8.36) is just another way of writing (3.38), where the replaceive mass

$$m = 4\pi R_0^3 \rho, \quad (8.37)$$

the linear angular resonance frequency

$$\omega_0 = \left( \frac{1}{R_0 \sqrt{\rho}} \right) \sqrt{3\gamma \left( p_0 - p_v + \frac{2\sigma}{R_0} \right) + p_v - \frac{2\sigma}{R_0} - \frac{4\eta^2}{\rho R_0^2}}, \quad (8.38)$$

and the (viscous) damping

$$2\zeta = \frac{16\pi\eta R_0}{m\omega_0} = \frac{4\eta}{\rho\omega_0 R_0^2}. \quad (8.39)$$

The damping of a bubble pulsation is determined by the acoustic radiation, the heat conduction, and the liquid viscosity. For microbubbles under sonication at typical medical frequencies  $> 1$  MHz, viscous damping is dominant, as is evident from (4.147). For an encapsulated microbubble, the presence of

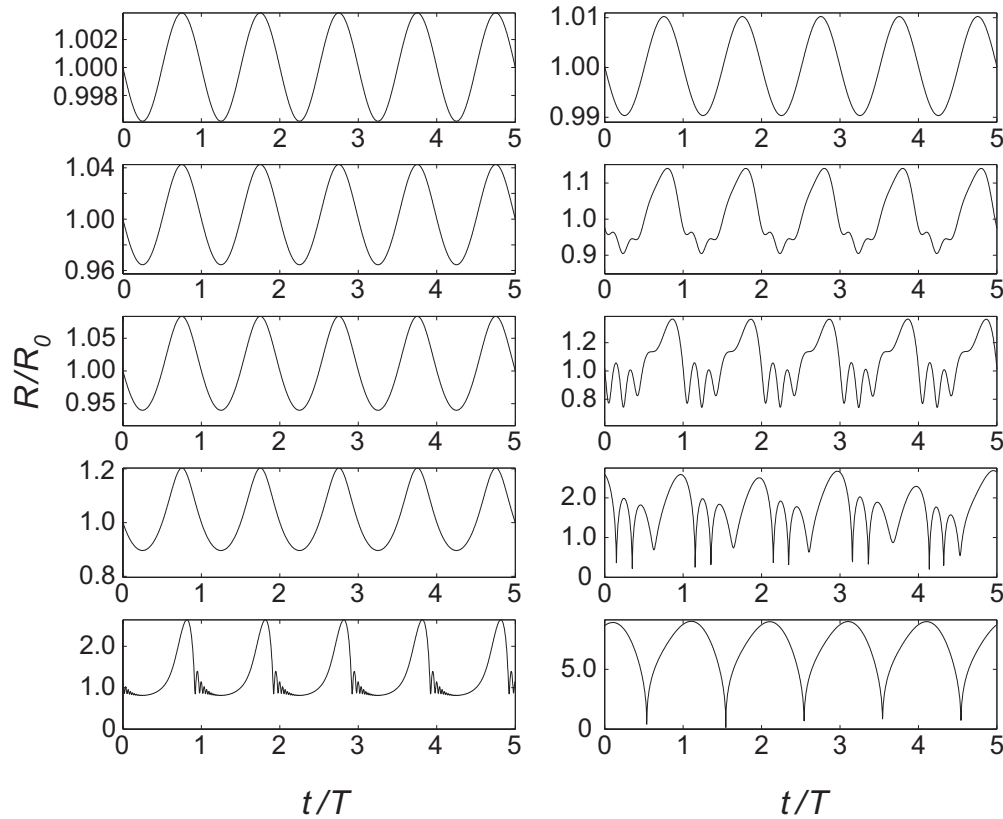


Figure 8.3: Simulated radius–time curves (radius  $R$  normalised by equilibrium radius  $R_0$ , time  $t$  normalised by period  $T$ ) of ultrasound contrast microbubbles with  $0.55\ \mu\text{m}$  (*left column*) and  $2.3\ \mu\text{m}$  (*right column*) equilibrium radii. The modelled ultrasound field was a continuous sine wave with a frequency of  $0.5\ \text{MHz}$  and acoustic amplitudes corresponding to (top–bottom)  $\text{MI} = 0.01, 0.10, 0.18, 0.35,$  and  $0.80$ . Reprinted with permission from Postema M, Gilja OH. Ultrasound-directed drug delivery. *Curr Pharm Biotechnol* **2007** 8:355–361.

a shell has to be taken into account, by adding an extra damping parameter  $\zeta_s$ . From (3.63) we know that the excursion of a forced damped harmonic oscillator has a phase angle difference  $\phi$  with the driving field. Figure 8.4 shows three curves of the phase angle differences ( $\phi + \pi$ ) between a damped radially oscillating bubble and an incident 2-MHz sound field, as a function of  $R_0$ . The curves have been computed for a free microbubble, a SonoVue<sup>TM</sup> contrast microbubble, and an Albunex<sup>®</sup> contrast microbubble. With in-

creasing shell stiffness, the bubble resonance size increases. At resonance, the bubble oscillates  $\frac{3}{2}\pi$  rad out of phase with the sound field. For bubble greater than resonance, the phase angle difference approaches  $2\pi$  rad, so that the bubble oscillates in phase with the sound field. Below resonance size, the phase difference is still greater than  $\pi$ , and approaches  $\frac{3}{2}\pi$  for  $R_0$  much smaller than resonance size. Since the damping due to the liquid viscosity  $\zeta_v \propto R^{-2}$ , the phase difference approaches  $\frac{3}{2}\pi$  for a free bubble radius  $R_0 \ll 1\ \mu\text{m}$ . The approach to  $\frac{3}{2}\pi$  below the minimum value of the phase difference is stronger with the contrast bubbles, because  $\zeta_s \propto R^{-3}$ . As the damping becomes greater, the phase transition around resonance becomes less abrupt, as Figure 8.4 demonstrates.<sup>1</sup>

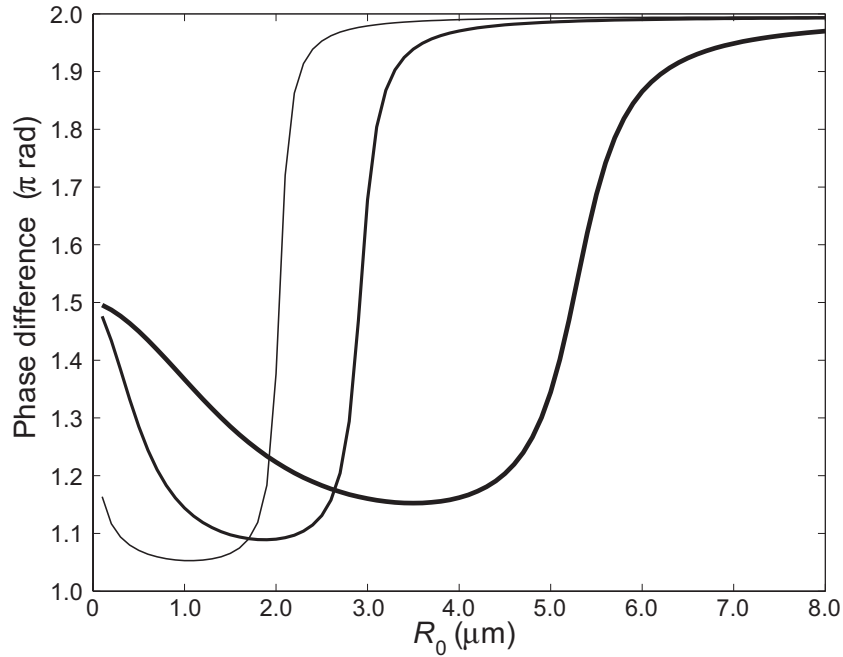


Figure 8.4: Phase angle difference ( $\phi + \pi$ ) between a damped radially oscillating bubble and an incident 2-MHz sound field, as a function of equilibrium radius  $R_0$ . The thin line represents a free bubble, the medium line a SonoVue<sup>TM</sup> microbubble, and the thickest line an Albunex<sup>®</sup> microbubble.

The spherically symmetric oscillating behaviour of ultrasound contrast agent microbubbles has been described with models based on the Rayleigh–

<sup>1</sup>Postema M, Schmitz G. Ultrasonic bubbles in medicine: influence of the shell. *Ultrason Sonochem* **2007** 14:438–444.

Plesset equation, modified for the presence of an encapsulating shell. Generally, the presence of blood has a relatively small effect on bubble dynamics. To give an indication of the vast amount of existing models: Qin *et al.* defined 16 separate dynamic bubble model classes.<sup>2</sup> The reason for the high number of existing models is the fact that most physical properties of encapsulated microbubbles cannot actually be measured, so that pseudo-material properties have to be chosen when predicting ultrasound contrast agent microbubble behaviour. Examples of such pseudo-material properties are shell elasticity parameters and shell friction parameters.

If the ultrasonic driving pressure is sufficiently high, the nonlinear microbubble response results in harmonic dispersion, which not only produces harmonics with frequencies that are integer multiples of  $\omega$  (superharmonics) but also subharmonics with frequencies less than  $\omega$  of the form  $m\omega/n$ , where  $\{m, n\} \in \mathbb{N}$ .

## 8.7 Disruption

At low acoustic amplitudes (mechanical index  $MI < 0.1$ ), microbubbles pulsate linearly. At high amplitudes ( $MI > 0.6$ ), their elongated expansion phase is followed by a violent collapse. During the collapse phase, when the kinetic energy of the bubble surpasses its surface energy, a bubble may fragment into a number of smaller bubbles. Fragmentation has been exclusively observed with contrast agents with thin, elastic shells. Fragmentation is the dominant disruption mechanism for these bubbles.

During the initial part of the collapse, the acceleration  $\ddot{R}$  is negative. This sign changes as the gas inside the bubble begins to be compressed, and the rebound begins. Provided that surface instabilities have grown big enough to allow for break-up, microbubble fragmentation has been expected and observed close to this moment, when  $\ddot{R} = 0$ . This has been confirmed by means of high-speed photography. The occurrence of fragmentation has been associated with inertial cavitation.

The number of fragments,  $N$ , into which a microbubble breaks up, is related to the dominant spherical harmonic oscillation mode  $n$  by<sup>3</sup>

$$N \approx n^3. \quad (8.40)$$

---

<sup>2</sup>Qin S, Caskey CF, Ferrara KW. Ultrasound contrast agent microbubbles in imaging and therapy: physical principles and engineering. *Phys Med Biol* **2009** 54:R27–R57.

<sup>3</sup>Brennen CE. Fission of collapsing cavitation bubbles. *J Fluid Mech* **2002** 472:153–166.

Mode 2 oscillations have been observed with lipid-encapsulated microbubbles, leading to fragmentation into 8 newly formed microbubbles.

Let us consider a single spherically symmetric microbubble with an inner radius  $R_i$  and an outer radius  $R$ , a shell density  $\rho_s$ , negligible translation, in an infinite fluid with density  $\rho$ . The kinetic energy of such a microbubble can be approximated by

$$E_k \approx 2\pi \rho R^3 \dot{R}^2 + 2\pi \rho_s R_i^3 \dot{R}_i^2 \left(1 - \frac{R_i}{R}\right). \quad (8.41)$$

Knowing that, for microbubbles with monolayer lipid shells,  $\frac{R_i}{R} < 0.01$  and  $\rho_s = 1.15 \times 10^3 \text{ kg m}^{-3}$ , and for blood,  $\rho = 1.05 \times 10^3 \text{ kg m}^{-3}$ , (8.41) can be reduced to (8.20).

The surface free energy  $E_s$  of a single encapsulated bubble is given by

$$E_s = 4\pi R_i^2 \sigma_1 + 4\pi R^2 \sigma_2, \quad (8.42)$$

where  $\sigma_1$  and  $\sigma_2$  denote the surface tension coefficient for the inner and outer interface, respectively. For our microbubbles with monolayer lipid shells, we consider a single interface model, using the effective surface tension  $\sigma$ :

$$\sigma = \sigma_1 + \sigma_2. \quad (8.43)$$

After fragmentation, the resulting microbubble fragments contain more surface free energy  $\sum_i E_{f,i}$  than the single bubble prior to fragmentation:

$$\sum_{i=1}^N E_{f,i} \approx \frac{4}{3}\pi R_{f,m}^2 \sigma N \approx \frac{4}{3}\pi R^2 \sigma N^{\frac{1}{3}} = N^{\frac{1}{3}} E_s, \quad (8.44)$$

where  $R_{f,m}$  is the mean fragment radius. Neglecting the elastic energy of the shell and the internal energy of the gas core, it can be assumed that fragmentation will only occur if:

$$E_k > \sum_{i=1}^N E_{f,i} - E_s. \quad (8.45)$$

Although asymmetric shape bubble oscillations have been observed, within the size range of ultrasound contrast agent bubbles, spherical harmonic modes higher than 2 can be neglected.

For microbubbles of radius  $R_0$  with a thick, stiff shell, such as Quantison<sup>TM</sup>,  $\max(R(t)) \ll R_0$ . Thick-shelled bubbles have demonstrated gas release during a high-amplitude ultrasonic cycle. The increased pressure difference between the inside and outside of the bubble during the expansion phase of the

wave causes the shell to be stretched across the critical deformation, resulting in its mechanical cracking. The released bubble has an oscillation amplitude much higher than an encapsulated bubble of the same size.

Figure 8.5 shows the ultrasound-induced release of gas from an albumin-encapsulated microbubble, driving the bubble at 0.5 MHz with a peak-negative acoustic pressure of 0.8 MPa.<sup>4</sup> The frames cover one full ultrasonic cycle ( $2\ \mu\text{s}$ ). This acoustic pressure is well within the clinical diagnostic range. Gas is seen to escape from the thick-shelled microbubble with a  $4.3\ \mu\text{m}$  diameter in the third frame, in the beginning of the rarefaction phase of the ultrasound. The shell itself is too rigid to expand. The released gas expands to a diameter of  $12.3\ \mu\text{m}$  in the eighth frame, after which it contracts. In the eleventh frame, the free gas microbubble, which has been subjected to motion blur, appears to be detached from the encapsulated microbubble. In the twelfth frame, the gas is hardly visible, owing to the compression phase of the ultrasound.

On the contrary, microbubbles with a thin, highly elastic monolayer lipid shell, like SonoVue<sup>TM</sup>, have been observed to expand to more than ten-fold their initial surface areas during rarefaction. The shell behaves like an elastic membrane that ruptures under relatively small strain. By the time of maximal expansion, therefore, the shell has ruptured, leaving newly formed clean free interfaces.

## 8.8 Diffusion

In a steady fluid, gas diffusion is given by Fick's law:

$$\frac{\partial C}{\partial t} = D \left( \frac{\partial^2 C}{\partial r^2} + \frac{2}{r} \frac{\partial C}{\partial r} \right), \quad (8.46)$$

where  $C$  is the mass concentration of the dissolved gas and  $D$  is the dissolution constant. We introduce

$$u(r, t) = r (C - C_s) \quad (8.47)$$

and the boundary condition

$$u(r, 0) = r (C_i - C_s), \quad (8.48)$$

---

<sup>4</sup>Postema M, Bouakaz A, Versluis M, de Jong N. Ultrasound-induced gas release from contrast agent microbubbles. *IEEE Trans Ultrason Ferroelectr Freq Control* **2005** 52:1035–1041.

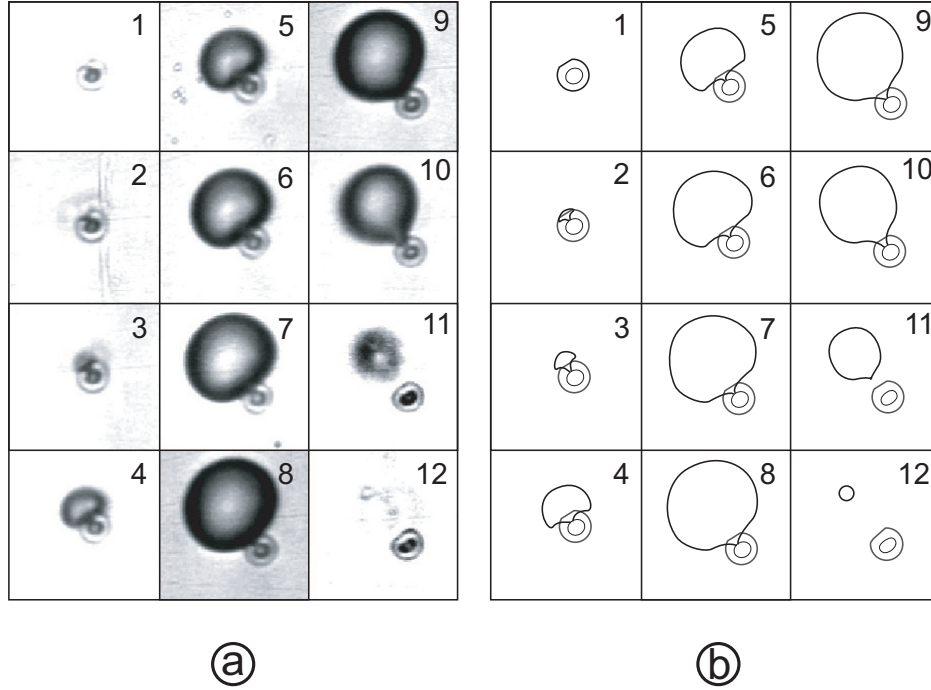


Figure 8.5: Gas release from the upper left of a Quantisium™ microbubble during a single ultrasonic cycle (a), and a schematic representation thereof (b). During the rarefaction phase (starting frame 2), gas escapes until it reaches a maximum (frame 8). During the subsequent contraction, the free gas bubble is seen detached from the shell (frames 11 and 12). Each frame corresponds to a  $19 \times 19 (\mu\text{m})^2$  area. Inter-frame times are  $0.1 \mu\text{s}$ . Reprinted with permission from Postema M, van Wamel A, ten Cate FJ, de Jong N. High-speed photography during ultrasound illustrates potential therapeutic applications of microbubbles. *Med Phys* **2005** 32:3707–3711.

where  $C_i$  is the initial mass concentration of the dissolved gas and  $C_s$  is the saturation concentration in the liquid at the bubble wall. Then,

$$\frac{\partial u}{\partial t} = D \frac{\partial^2 u}{\partial r^2}. \quad (8.49)$$

The solution of this ordinary differential equation is

$$u(r, t) = u(r, 0) \operatorname{erf}(z), \quad (8.50)$$

where

$$z = \frac{r}{2\sqrt{Dt}}. \quad (8.51)$$

The error function  $\text{erf}(z)$  is defined by

$$\text{erf}(z) = \frac{2}{\sqrt{\pi}} \int_0^z e^{-\xi^2} d\xi \quad (8.52)$$

and can be written as an asymptotic series

$$\text{erf}(z) = 1 - \frac{e^{-z^2}}{\sqrt{\pi}} \sum_{n=0}^{\infty} \frac{(-1)^n (2n-1)!!}{2^n} z^{-(2n+1)} = 1 - \frac{e^{-z^2}}{\sqrt{\pi}} \left( z^{-1} - \frac{z^{-3}}{3} + \dots \right). \quad (8.53)$$

Substituting for  $u(r, 0)$ , (8.50) now becomes

$$u(r, t) = \frac{2r(C_i - C_s)}{\sqrt{\pi}} \int_0^{\frac{r}{2\sqrt{Dt}}} e^{-\xi^2} d\xi. \quad (8.54)$$

Using the asymptotic series for  $\text{erf}(z)$  and the Taylor series for  $e^z$ , it follows that, at  $r = R$ ,

$$\left( \frac{\partial u}{\partial r} \right)_R = (C_i - C_s) \left( 1 + \frac{R}{\sqrt{\pi Dt}} \right) \quad (8.55)$$

and, consequently,

$$\left( \frac{\partial C}{\partial r} \right)_R = (C_i - C_s) \left( \frac{1}{R} + \frac{1}{\sqrt{\pi Dt}} \right). \quad (8.56)$$

At the bubble wall, the mass flow through the surface equals the diffusion:

$$D \left( \frac{\partial C}{\partial r} \right)_R = \frac{1}{4\pi R^2} \frac{dm}{dt} = \frac{1}{4\pi R^2} \frac{d}{dt} \left( \frac{4}{3} \pi R^3 \rho_g \right) \quad (8.57)$$

or

$$4\pi R^2 \dot{R} \rho_g = 4\pi R^2 D \left( \frac{\partial C}{\partial r} \right)_R \quad (8.58)$$

where  $\rho_g$  is the density of the gas. Substituting (8.56) yields the bubble wall velocity during dissolution:

$$\dot{R} = \frac{D(C_i - C_s)}{\rho_g} \left( \frac{1}{R} + \frac{1}{\sqrt{\pi Dt}} \right). \quad (8.59)$$

In this equation,  $\rho_g$  is a function of  $R$ . Combining (4.22) and (8.4) rephrases the ideal gas law for a gas bubble:

$$p_0 + \frac{2\sigma}{R} = \frac{\rho_g \mathcal{R} \mathcal{T}}{M}, \quad (8.60)$$

so that  $\rho_g$  is expressed in terms of known parameters:

$$\rho_g(R) = \frac{M}{\mathcal{RT}}(p_0 - p_v) + \frac{2M\sigma}{\mathcal{RT}} \frac{1}{R} = \rho_g(\infty) + \frac{2M\sigma}{\mathcal{RT}} \frac{1}{R}, \quad (8.61)$$

where  $\rho_g(\infty)$  is the density of the gas under the same conditions of pressure and temperature with a gas–liquid interface of zero curvature.<sup>5</sup> Substituting (8.61) into (8.57) and computing the mass diffusion rephrases (8.59) as

$$\dot{R} = \frac{D(C_i - C_s)}{\rho_g(\infty) + \frac{4}{3} \frac{M\sigma}{\mathcal{RT}} \frac{1}{R}} \left( \frac{1}{R} + \frac{1}{\sqrt{\pi Dt}} \right) \quad (8.62)$$

or

$$\dot{R} = \frac{D\mathcal{RT}(C_i - C_s)}{M} \frac{1}{p_0 - p_v + \frac{4}{3} \frac{\sigma}{R}} \left( \frac{1}{R} + \frac{1}{\sqrt{\pi Dt}} \right). \quad (8.63)$$

The concentration of gas at the bubble wall  $C_s$  is related to the internal gas pressure by

$$C_s = k_g^{-1} p_g = k_g^{-1} \left( p_0 - p_v + \frac{2\sigma}{R} \right), \quad (8.64)$$

where  $k_g$  is Henry's constant defined in terms of the mass concentration of the gas. The saturation concentration of the gas is, by definition,<sup>6</sup>

$$C_0 = k_g^{-1} p_0. \quad (8.65)$$

Hence, the concentration of gas at the bubble wall is related to the saturation concentration in the liquid by

$$C_s = C_0 \left( 1 - \frac{p_v}{p_0} + \frac{2\sigma}{p_0 R} \right). \quad (8.66)$$

Equation (8.63) now reduces to

$$\dot{R} = \frac{D\mathcal{RT}C_0}{Mp_0} \left( \frac{\frac{C_i}{C_0} - 1 + \frac{p_v}{p_0} - \frac{2\sigma}{Rp_0}}{1 - \frac{p_v}{p_0} + \frac{4}{3} \frac{\sigma}{Rp_0}} \right) \left( \frac{1}{R} + \frac{1}{\sqrt{\pi Dt}} \right), \quad (8.67)$$

which can be simplified to

$$\dot{R} = DL \left( \frac{\frac{C_i}{C_0} - 1 + \frac{p_v}{p_0} - \frac{2\sigma}{Rp_0}}{1 - \frac{p_v}{p_0} + \frac{4}{3} \frac{\sigma}{Rp_0}} \right) \left( \frac{1}{R} + \frac{1}{\sqrt{\pi Dt}} \right), \quad (8.68)$$

<sup>5</sup>Epstein PS, Plesset MS. On the stability of gas bubbles in liquid–gas solutions. *J Chem Phys* **1950** 18:1505–1509.

<sup>6</sup>Eller A, Flynn AG. Rectified diffusion during nonlinear pulsations of cavitation bubbles. *J Acoust Soc Am* **1965** 37:493–503.

where  $L$  is Ostwald's solubility coefficient.<sup>7</sup> If a hydrostatic overpressure  $\Delta p$  is introduced, the dissolution can be readily derived in a similar fashion:

$$\dot{R} = DL \left( \frac{\frac{C_i}{C_0} - 1 + \frac{p_v}{p_0} - \frac{\Delta p}{p_0} - \frac{2\sigma}{Rp_0}}{1 - \frac{p_v}{p_0} + \frac{\Delta p}{p_0} + \frac{4}{3} \frac{\sigma}{Rp_0}} \right) \left( \frac{1}{R} + \frac{1}{\sqrt{\pi Dt}} \right). \quad (8.69)$$

Figure 8.6 shows diameter–time curves of free dissolving nitric oxide gas microbubbles at two different ambient pressures. The dissolution process of

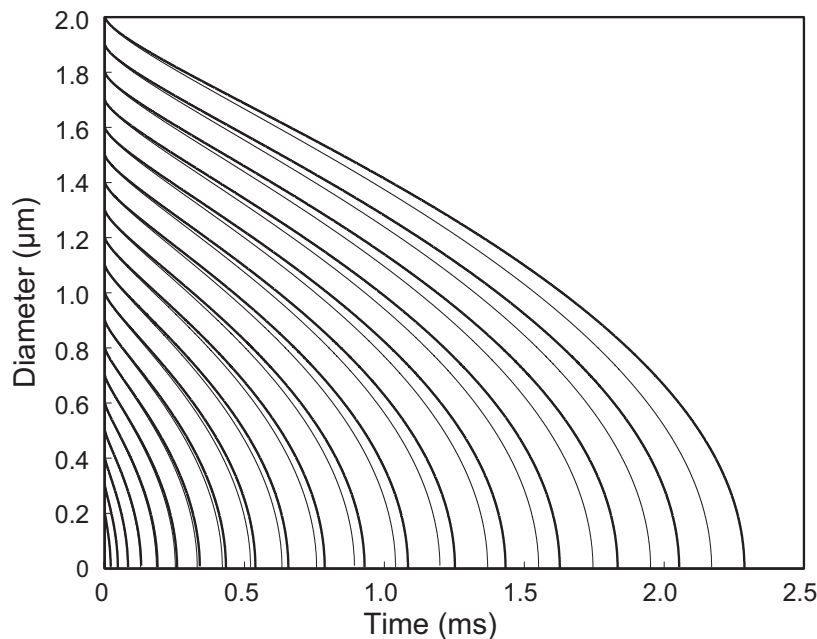


Figure 8.6: Diameter–time curves of dissolving nitric oxide gas bubbles at atmospheric pressure (bold lines) and 100 mmHg overpressure (thin lines), respectively. Reprinted with permission from Postema M, Bouakaz A, ten Cate FJ, Schmitz G, de Jong N, van Wamel A. Nitric oxide delivery by ultrasonic cracking: some limitations. *Ultrasonics* **2006** 44:e109–e113.

a 2- $\mu\text{m}$  microbubble takes less than 2.5 ms. Increasing the ambient pressure slightly decreases the dissolution times.

<sup>7</sup>Bouakaz A, Frinking PJA, de Jong N, Bom N. Noninvasive measurement of the hydrostatic pressure in a fluid-filled cavity based on the disappearance time of micrometer-sized free gas bubbles. *Ultrasound Med Biol* **1999** 25:1407–1415.

## 8.9 Radiation forces

### 8.9.1 Travelling sound wave

Consider a pressure gradient  $\nabla p$  across a bubble of volume  $V$ . The force acting on the bubble must be

$$F = -V\nabla p. \quad (8.70)$$

In an acoustic field, the pressure gradient constantly changes. Hence, we consider the average force acting on the bubble, following the analysis by Leighton:<sup>8</sup>

$$\langle F \rangle = -\langle V\nabla p \rangle. \quad (8.71)$$

Now, consider a plane single-frequency (monotonous) progressive wave in the  $x$ -direction, for which the pressure deviation from the ambient constant value is described by (4.35):

$$p = P_A \cos(\omega t - kx) \quad (8.72)$$

and

$$\nabla p = -kP_A \sin(\omega t - kx), \quad (8.73)$$

where  $P_A$  is the acoustic pressure amplitude,  $k$  is the wave number, and  $\omega$  is the angular driving frequency. At small acoustic amplitudes, a bubble oscillates linearly:

$$R(t) = R_0 - \xi \cos(\omega t - kx - \phi), \quad (8.74)$$

where  $\xi$  is the bubble oscillation amplitude and  $\phi$  is the phase difference between the sound field and the bubble. The volumetric change is then approximated by

$$\begin{aligned} V(t) &= \frac{4}{3}\pi [R_0 - \xi \cos(\omega t - kx - \phi)]^3 \\ &= \frac{4}{3}\pi [R_0^3 - 3R_0^2\xi \cos(\omega t - kx - \phi) + 3R_0\xi^2 \cos^2(\omega t - kx - \phi) \\ &\quad - \xi^3 \cos^3(\omega t - kx - \phi)] \\ &\approx V_0 \left[ 1 - \frac{3\xi}{R_0} \cos(\omega t - kx - \phi) \right]. \end{aligned} \quad (8.75)$$

Hence, the average force acting on the bubble is

$$\langle F \rangle = -\left\langle V_0 k P_A \left[ 1 - \frac{3\xi}{R_0} \cos(\omega t - kx - \phi) \right] \sin(\omega t - kx) \right\rangle. \quad (8.76)$$

---

<sup>8</sup>Leighton TG. *The Acoustic Bubbles*. London: Academic Press **1994**.

Making use of  $\sin A \cos(A + B) = \frac{1}{2} \sin 2A \cos B - \sin^2 A \sin B$ , this becomes

$$\begin{aligned} \langle F \rangle = -V_0 k P_A (\langle \sin(\omega t - kx) \rangle + \frac{3\xi}{R_0} \langle \sin^2(\omega t - kx) \sin \phi \rangle \\ + \langle \sin(\omega t - kx) \cos(\omega t - kx) \cos \phi \rangle). \end{aligned} \quad (8.77)$$

The uneven terms are averaged out, whereas  $\langle \sin^2 A \rangle = \frac{1}{2}$ , so that

$$\langle F \rangle = \frac{3V_0 k P_A}{2} \frac{\xi}{R_0} \sin \phi. \quad (8.78)$$

Substituting (3.63) for  $\phi$  and taking into account that  $\sin \arctan x = \frac{x}{\sqrt{1+x^2}}$  gives:

$$\langle F \rangle = \frac{3V_0 k P_A}{2} \frac{\xi}{R_0} \frac{2\zeta \frac{\omega}{\omega_0}}{\sqrt{\left(1 - \left(\frac{\omega}{\omega_0}\right)^2\right)^2 + \left(2\zeta \frac{\omega}{\omega_0}\right)^2}}. \quad (8.79)$$

This force, acting in the direction of the sound field, is called the primary radiation force.

## 8.9.2 Standing sound wave

Consider a bubble in a standing sound wave

$$p = 2P_A \cos \omega t \cos kx \quad (8.80)$$

and

$$\nabla p = -kP_A \sin(\omega t - kx). \quad (8.81)$$

At small acoustic amplitudes, the radius is then given by

$$R(t) = R_0 - \xi \cos kx \cos(\omega t - \phi). \quad (8.82)$$

Analogous to (8.75), the volumetric change is approximated by

$$V(t) \approx V_0 \left[ 1 - \frac{3\xi}{R_0} \cos kx \cos(\omega t - \phi) \right]. \quad (8.83)$$

Consequently, the average force acting on the bubble is

$$\langle F \rangle = - \left\langle 2V_0 k P_A \left[ 1 - \frac{3\xi}{R_0} \cos kx \cos(\omega t - \phi) \right] \sin kx \cos \omega t \right\rangle. \quad (8.84)$$

Again, the uneven terms are averaged out, so that

$$\langle F \rangle = \frac{3V_0 k P_A}{2} \frac{\xi}{R_0} \sin 2kx \cos \phi. \quad (8.85)$$

Substituting (3.63) for  $\phi$  and taking into account that  $\cos \arctan x = \frac{1}{\sqrt{1+x^2}}$  gives

$$\langle F \rangle = \frac{3V_0 k P_A \sin 2kx}{2} \frac{\xi}{R_0} \frac{1 - \left(\frac{\omega}{\omega_0}\right)^2}{\sqrt{\left(1 - \left(\frac{\omega}{\omega_0}\right)^2\right)^2 + \left(2\zeta \frac{\omega}{\omega_0}\right)^2}}. \quad (8.86)$$

This force, acting in the direction of the nodes and anti-nodes of the sound field, is called the primary Bjerknes force.

### 8.9.3 Radiation forces between bubbles

Consider an object in a sound field that causes a fluid acceleration  $\dot{v}$  at the position of a bubble of interest. Defining  $\dot{u}$  as the acceleration of the bubble, the net acceleration of the bubble relative to the fluid is  $\dot{u} - \dot{v}$ . This relative acceleration causes a drag force on the bubble  $-\frac{1}{2}\rho V (\dot{u} - \dot{v})$ , where  $\frac{1}{2}\rho V$  is the apparent mass of a moving bubble. Following Leighton's derivation, the net force on the bubble is

$$F = \rho V \dot{v} - \frac{1}{2}\rho V (\dot{u} - \dot{v}) = \rho_g(t) V \dot{u}, \quad (8.87)$$

from which an expression for  $\dot{u}$  immediately follows:

$$\dot{u} = \frac{3V\dot{v}}{V + 2V\frac{\rho_g}{\rho}}. \quad (8.88)$$

If the mass of the gas inside the bubble is constant,

$$\rho_g V = \rho_{0,g} V_0, \quad (8.89)$$

where  $\rho_{0,g}$  is the density of the gas bubble in quasi-equilibrium. We assume the bubble oscillates linearly according to

$$V(t) = V_0 - \Delta V \cos \omega t, \quad (8.90)$$

where  $\Delta V = 4\pi R^2 \xi$ . We substitute this for  $V$  and the density ratio  $f$  for  $\frac{\rho_{0,g}}{\rho}$  in (8.88):

$$\frac{\dot{u}}{\dot{v}} = \frac{3(V_0 - \Delta V \cos \omega t)}{(1 + 2f)V_0 - \Delta V \cos \omega t}. \quad (8.91)$$

Using  $\frac{1}{1-x} = 1 + x + x^2 + x^3 + \dots$ , this can be simplified to

$$\begin{aligned} \frac{\dot{v}}{v} &= \frac{3}{1+2f} \left( 1 - \frac{\Delta V \cos \omega t}{V_0} \right) \left( 1 + \frac{\Delta V \cos \omega t}{(1+2f)V_0} \right) \\ &\approx \frac{3}{1+2f} \left( 1 - \frac{2f}{1+2f} \frac{\Delta V}{V_0} \cos \omega t \right). \end{aligned} \quad (8.92)$$

Now, consider that the object causing the fluid acceleration  $\dot{v}$  is a bubble “1” at distance  $r$  from the bubble of interest “2”. If  $V_1$  is the volume of bubble 1 at quasi-equilibrium,  $V_2$  is the volume of bubble 2 at quasi-equilibrium,  $\Delta V_1$  is the volumetric expansion amplitude of bubble 1, and  $\Delta V_2$  is the volumetric expansion amplitude of bubble 2, then, assuming small oscillation amplitudes, the instantaneous volume of bubble 1 is  $V_1 - \cos(\omega t + \phi)$  and the instantaneous volume of bubble of 2 is  $V_2 - \cos \omega t$ , where  $\phi$  is the difference in oscillation phase. We define  $\rho_1$  and  $\rho_2$  as the gas density at equilibrium of bubble 1 and 2, respectively. Similar to (8.87), the average force experienced by bubble 2 is

$$\langle F \rangle = \langle \rho V \dot{v} \rangle = \rho_2 V_2 \langle \dot{v} \rangle = \frac{3}{1+2f} \left\langle \dot{v} \rho_2 V_2 - \frac{6f}{(1+f)^2} \dot{v} \rho_2 \Delta V_2 \cos \omega t \right\rangle. \quad (8.93)$$

Considering that  $V_1 = \frac{4}{3}\pi R_1^3$  and that  $\dot{V}_1 = 4\pi R_1^2 \dot{R}_1$ , (8.18) can be rewritten in terms of  $V_1$ :

$$v = \frac{R_1^2 \dot{R}_1}{r^2} = \frac{\dot{V}_1}{4\pi r^2} = \frac{\omega \Delta V_1 \sin(\omega t + \phi)}{4\pi r^2}, \quad (8.94)$$

so that

$$\dot{v} = \frac{\omega^2 \Delta V_1 \cos(\omega t + \phi)}{4\pi r^2}. \quad (8.95)$$

Inserting this in (8.93) results in

$$\begin{aligned} \langle F \rangle &= \frac{3}{1+2f} \frac{\rho_2 \omega^2 \Delta V_1 V_2}{4\pi r^2} \langle \cos(\omega t + \phi) \rangle \\ &\quad - \frac{6f}{(1+f)^2} \frac{\rho_2 \omega^2 \Delta V_1 \Delta V_2}{4\pi r^2} \langle \cos \omega t \cos(\omega t + \phi) \rangle \\ &= -\frac{3f}{(1+2f)^2} \frac{\rho_2 \omega^2 \Delta V_1 \Delta V_2}{4\pi r^2} \cos \phi. \end{aligned} \quad (8.96)$$

This force is called the secondary radiation or secondary Bjerknes force. From (8.96), it immediately follows that bubbles that oscillate in phase ( $\phi = 0$ ) attract each other and that bubbles that oscillate out of phase ( $\phi = \pi$ ) repel each other.

## 8.10 Coalescence

To understand microbubble coalescence, one needs to comprehend the drainage of the liquid separating the bubble surfaces. Reynolds noted that the viscosity of a liquid can be determined by pressing two flat plates together, squeezing the liquid out, and measuring the drainage velocity.<sup>9</sup> Thus, he formulated an equation for the drainage velocity of a fluid between rigid surfaces. General theories on the coalescence of colliding bubbles and droplets have been based on liquid film drainage.<sup>10,11</sup> Droplet coalescence finds applications in fuel ignition research and aerosol studies, whereas the research on bubble coalescence focuses on thin film physics and foam stability. This Section explores ultrasound-induced coalescence of microbubbles. Controlled coalescence has potential applications in the clinical field.<sup>12</sup>

Theories on bubble coalescence are generally based on the collision of unencapsulated bubbles or droplets, approaching each other at constant velocity. During expansion, microbubbles may also come into contact with each other, resulting in coalescence or bounce. We discriminate the following stages in the coalescence mechanism, optically observed in Figure 8.7 and schematically represented in Figure 8.8. Initially, two bubbles approach collision while expanding (Figure 8.8(a)). Prior to contact, there may be a flattening of the adjacent bubble surfaces, trapping liquid in between (Figure 8.7(a), Figure 8.8(b)). This trapped liquid drains (Figure 8.7(b), Figure 8.8(c)) until the separation reaches a critical thickness. An instability mechanism results in rupture of the separation (Figure 8.8(d)) and the formation of a merged bubble (Figure 8.7(c)). After coalescence the resulting bubble will have an ellipsoidal shape (Figure 8.7(d), Figure 8.8(e)). Owing to surface tension, it will relax to a spherical shape. When the contact time is less than the time needed for film drainage, the bubbles bounce off each other.<sup>13</sup> We define bubble coalescence as the fusing of two or more bubbles

---

<sup>9</sup>Reynolds O. On the theory of lubrication and its application to Mr. Beauchamp Tower's experiments, including an experimental determination of the viscosity of olive oil. *Philos Trans Roy Soc A* **1886** 177:157–234.

<sup>10</sup>Kralchevsky PA, Danov KD, Ivanov IB. Thin liquid film physics. In: Prud'homme R, Khan S, eds., *Foams, Theory, Measurements and Applications*. New York: Marcel Dekker **1996** 1–98.

<sup>11</sup>Narsimhan G, Ruckenstein E. Structure, drainage, and coalescence of foams and concentrated emulsions. In: Prud'homme R, Khan S, eds., *Foams, Theory, Measurements and Applications*. New York: Marcel Dekker **1996** 99–187.

<sup>12</sup>Postema M, Marmottant, Lancée CT, Hilgenfeldt S, de Jong N. Ultrasound-induced microbubble coalescence. *Ultrasound Med Biol* **2004** 30:1337–1344.

<sup>13</sup>Chaudhari RV, Hofmann H. Coalescence of gas bubbles in liquids. *Rev Chem Eng* **1994** 10:131–190.

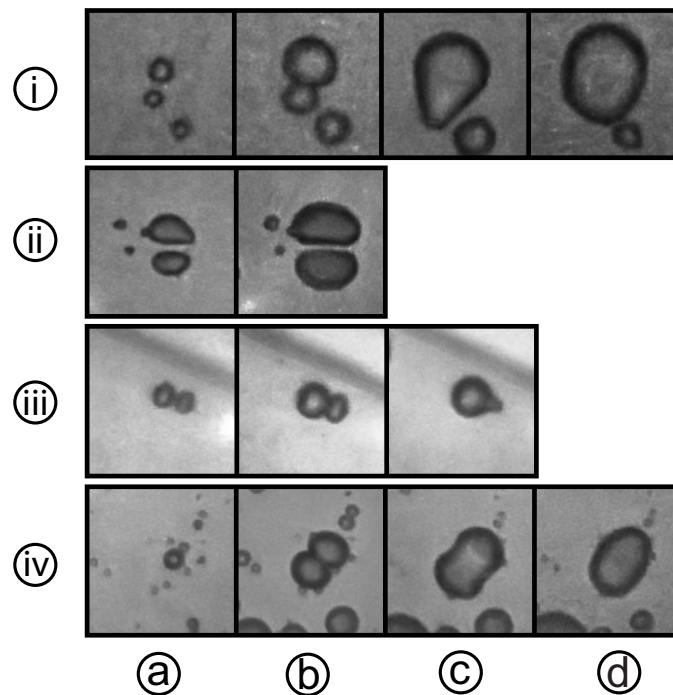


Figure 8.7: Optical images of stages of ultrasound-induced microbubble coalescence: (a) flattening of contact surfaces, (b) liquid film drainage, (c) forming of a merged bubble, (d) turning into an ellipsoidal bubble. Each frame in event (i) corresponds to a  $21 \times 21 (\mu\text{m})^2$  area. Each frame in events (ii)–(iv) corresponds to a  $30 \times 30 (\mu\text{m})^2$  area. Inter-frame times are  $0.33 \mu\text{s}$ . Reprinted with permission from Postema M, Marmottant P, Lancée CT, Hilgenfeldt S, de Jong N. Ultrasound-induced microbubble coalescence. *Ultrasound Med Biol* **2004** 30:1337–1344.

into a single bubble. The process begins with the flattening of the bubble surfaces and is considered finished when the resulting bubble has a spherical shape.

### 8.10.1 Flattening of the interface

Flattening of the opposing bubble surfaces occurs because the liquid inertia overcomes the capillary pressure, as described in earlier work on colliding bubbles with constant volumes. For colliding bubbles, flattening happens if

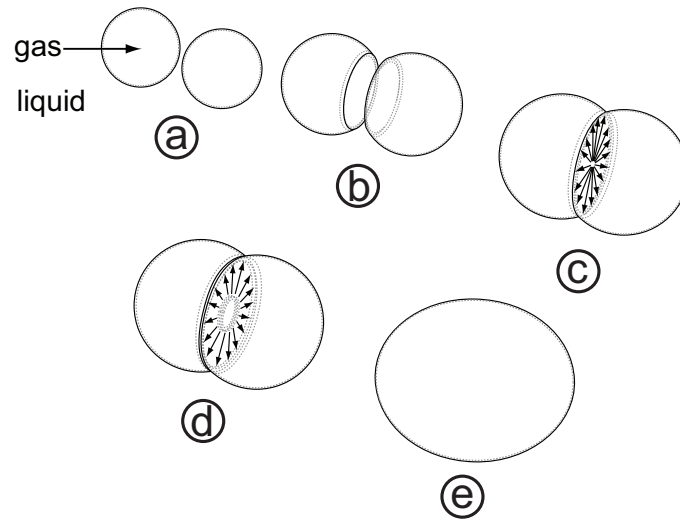


Figure 8.8: Schematic representation of stages of expanding bubble coalescence: (a) bubble collision, (b) flattening of contact surfaces, (c) liquid film drainage until a critical thickness (d), (e) film rupture, and (f) formation of an ellipsoidal bubble.

the bubble system has a Weber number  $We \gtrsim 0.5$ .<sup>14</sup> The Weber number for two colliding bubbles with radii  $R_1$  and  $R_2$ , respectively, is given by the inertial force relative to the surface tension force:

$$We = \frac{\rho u^2}{\frac{\sigma}{R_m}}, \quad (8.97)$$

where  $u$  is the relative approach velocity of the bubble walls,  $\rho$  is the fluid density,  $\sigma$  is the surface tension, and  $R_m$  is the mean bubble radius, which is defined by

$$\frac{2}{R_m} = \frac{1}{R_1} + \frac{1}{R_2}. \quad (8.98)$$

Consider the Weber number criterium for approaching walls of expanding bubbles. Then, for bubbles with a constant centre-to-centre distance,  $u = \dot{R}_1 + \dot{R}_2$ . If the Weber number is low, bubble coalescence will always occur, without flattening of the adjacent surfaces prior to contact. In the high Weber number regime, coalescence is determined by a second step, after flattening: film drainage.

<sup>14</sup>Duineveld PC. Bouncing and coalescence phenomena of two bubbles in water. In: Blake JR, Boulton-Stone JM, Thomas NH, eds., *Bubble Dynamics and Interface Phenomena*. Volume 23 of *Fluid mechanics and its applications*. Dordrecht: Kluwer Academic Publishers 1994 447–456.

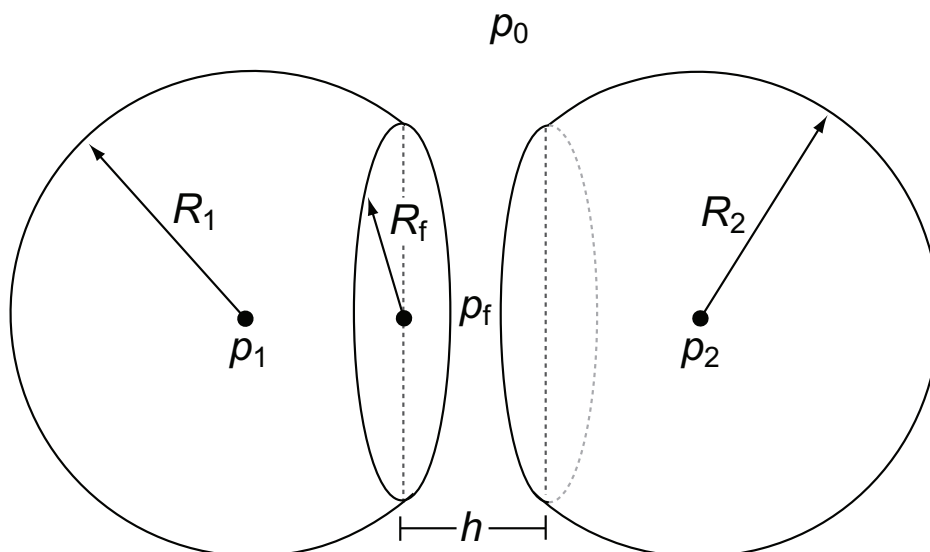


Figure 8.9: Schematic overview of variables used.

### 8.10.2 Film drainage

Consider two bubbles with radii  $R_1$  and  $R_2$ , and internal pressures  $p_1$  and  $p_2$ , respectively, assumed spherical everywhere with the exception of a flattened interface that separates them through a liquid film of thickness  $h$  (*cf.* Figure 8.9). The drainage rate of the liquid film depends on the difference  $(p+\Pi)$  between the film pressure  $p_f$  and the liquid ambient pressure  $p_0$ . Here,  $p$  is the difference in hydrodynamic pressure and  $\Pi$  is the disjoining pressure in the film. We estimate the pressure in the film by the mean of pressures  $p_1$  and  $p_2$ , since the parallel film surfaces lead to equal pressure differences towards both bubbles:

$$p + \Pi = p_f - p_0 = \frac{1}{2}(p_1 + p_2) - p_0 = \sigma \left( \frac{1}{R_1} + \frac{1}{R_2} \right) \equiv p_{LY}, \quad (8.99)$$

where  $p_{LY}$  is the Laplace–Young film pressure. The disjoining pressure begins to slow down film thinning when  $h$  drops below  $0.1 \mu\text{m}$ , and becomes the dominant pressure term (usually owing to Van der Waals forces) when  $h$  thins to about  $10 \text{ nm}$ .<sup>15</sup> The eventual coalescence of ultrasound contrast agent microbubbles is very fast compared with the film drainage time scales considered later. Therefore, we may neglect  $\Pi$  and take  $p$  equal to the Laplace–Young pressure for the films observed. As such, the pressure gradient determining the drainage velocity is independent of the ambient pressure.

<sup>15</sup>Marrucci G. A theory of coalescence. *Chem Eng Sci* **1969** 24:975–985.

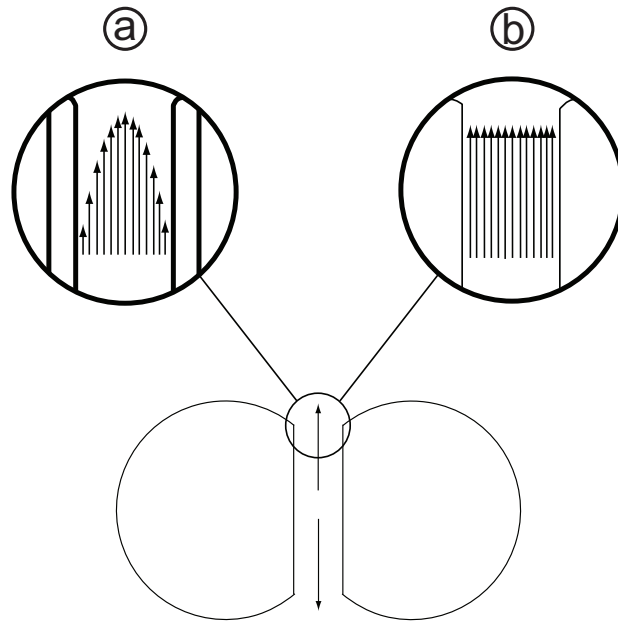


Figure 8.10: Schematic flow profiles between no-slip interfaces (a) and of free interfaces (b).

We choose an  $r$ - $z$  coordinate system such that the film is symmetric around the plane  $z = 0$  and the line  $r = 0$ , and that its boundaries are located at  $z = \pm\frac{1}{2}h$  and  $r = R_f$ . The Laplace–Young pressure gradient drives liquid out of the film. The radial velocity of the liquid is described by a combination of a plug flow (present without any resistance to flow) and a laminar flow profile (in  $z$ ) of Poiseuille type induced by resistance at the film interfaces.<sup>16</sup> The drainage of the liquid film can be parameterised by functions of these two contributions. Below, the two limiting cases of bubbles with no-slip interfaces and bubbles with free interfaces are analysed.

### 8.10.3 No-slip interfaces

In the presence of surfactant at sufficient surface concentration, the interfaces can be considered immobile (no-slip). In the case of no-slip interfaces, the interfacial tangential velocity is zero, so the plug flow contribution is zero, as shown in frame (a) of Figure 8.10.

<sup>16</sup>Klaseboer E, Chevaillier JP, Gourdon C, Masbernat O. Film drainage between colliding drops at constant approach velocity: experiments and modeling. *J Colloid Interf Sci* **2000** 229:274–285.

The film drainage velocity for rigid radial surfaces (disks) is given by the Reynolds equation:<sup>17</sup>

$$-\frac{\partial h}{\partial t} = \frac{2p h^3}{3\eta R_f^2}. \quad (8.100)$$

The drainage time,  $\tau_d$ , between the initial film thickness  $h_i$  and the critical film thickness  $h_c$  can be determined by integration of (8.100):

$$\int_{h_i}^{h_c} -\frac{dh}{h^3} = \int_0^{\tau_d} \frac{2p}{3\eta R_f^2} dt. \quad (8.101)$$

Flattening takes place when

$$\dot{R}_1 + \dot{R}_2 \gg \frac{\partial h}{\partial t}, \quad (8.102)$$

whereas the flat film drainage happens in the next stage, when

$$\dot{R}_1 \approx \dot{R}_2 \approx 0. \quad (8.103)$$

Thus, during drainage, we may take  $p$  and  $R_f$  constant over time. Then we obtain

$$\tau_d = \frac{3\eta R_f^2}{4p h_c^2} \left(1 - \frac{h_c^2}{h_i^2}\right). \quad (8.104)$$

If  $h_c^2 \ll h_i^2$  the drainage time can be approximated by

$$\tau_d \approx \frac{3\eta R_f^2}{4p h_c^2}. \quad (8.105)$$

#### 8.10.4 Free interfaces

In the case of free interfaces, the Poiseuille contribution to the drainage flow becomes negligible, and the drainage is inertial, as shown in frame (b) of Figure 8.10. The film drainage velocity for free radial surfaces is given by the equation<sup>18</sup>

$$-\frac{\partial h}{\partial t} = \sqrt{\frac{8p}{\rho}} \frac{h}{R_f}. \quad (8.106)$$

<sup>17</sup>Sheludko A. Thin liquid films. *Advan Colloid Interf Sci* **1967** 1:391–464.

<sup>18</sup>Kirkpatrick RD, Lockett MJ. The influence of approach velocity on bubble coalescence. *Chem Eng Sci* **1974** 29:2363–2373.

Note that the viscous term is absent. Similarly to the no-slip case, making the same quasi-static assumptions with regards to  $p$  and  $R_f$ , the drainage time can be approximated by

$$\tau_d \approx R_f \sqrt{\frac{\rho}{8p}} \log \left( \frac{h_i}{h_c} \right). \quad (8.107)$$

These drainage times are much smaller than those for the no-slip situation, and depend only logarithmically on both the initial and the critical film thickness.

### 8.10.5 Film rupture

The disjoining pressure induces rupture by amplifying surface perturbations. These are initialised by either thermal fluctuations or by capillary waves.<sup>19</sup> For thermal perturbations of a gas bubble in the micrometre range, the initial perturbation will be on the order of  $\sqrt{\frac{kT}{\sigma}}$ , where  $k$  is Boltzmann's constant and  $T$  is the absolute temperature, in our situation approximately 300 K. Hence, the initial thermal perturbation is lower than 1 nm.

A film gradually thins to a critical thickness at which it either ruptures due to a local instability or at which it attains an equilibrium thickness. These critical thicknesses dependent of surfactant concentration and film radius. They lie in the range  $20 \text{ nm} < h_c < 40 \text{ nm}$  for film radii  $60 \mu\text{m} < R_f < 160 \mu\text{m}$ .<sup>20</sup>

For ultrasound contrast agent film radii ( $R_f < 10 \mu\text{m}$ ), we may assume critical thicknesses around 10 nm, knowing that below 10 nm Van der Waals forces become very strong and rapid rupture of the film (and thus coalescence) ensues. Because of the weak dependence on film thickness, predictions from (8.107) for coalescence time scales can be quite accurate even without precise knowledge of  $h_i$  and  $h_c$ .

---

<sup>19</sup>Sharma A, Ruckenstein E. Critical thickness and lifetimes of foams and emulsions: role of surface wave-induced thinning. *J Colloid Interf Sci* **1987** 119:14–29.

<sup>20</sup>Angarska JK, Dimitrova BS, Danov KD, Kralchevsky PA, Ananthapadmanabhan KP, Lips A. Detection of the hydrophobic surface force in foam films by measurements of the critical thickness of film rupture. *Langmuir* **2004** 20:1799–1806.

## 8.11 Jetting

The jetting phenomenon for cavitation bubbles can be described as follows.<sup>21</sup> Consider an oscillation bubble. Let's define an infinite boundary to the right-hand side of the bubble. During sonication, at the moment of maximal expansion (*cf.* Figure 8.11b1), the pressure inside the bubble is much lower than the ambient pressure, causing the bubble to collapse. The radial water flow is retarded by the boundary. Therefore, the pressure at the right bubble wall is less than the pressure at the right wall during the whole collapse phase and the bubble becomes elongated perpendicular to the boundary. The pressure gradient leads to different accelerations of the left and right bubble walls and therefore to a movement of the centre of the bubble towards the boundary during collapse. As the bubble collapses, the fluid volume to the left of the bubble is accelerated and focussed, leading to the formation of a liquid jet directed towards the boundary. This jet hits the right-hand-side bubble wall, causing a funnel-shaped protrusion (*cf.* Figure 8.11b2) and finally impacts the boundary.

Empirical relations exist between bubble radius, jet length, and pressure at the tip of jets. The radius of the jet  $R_j$  is related to the radius of the bubble on the verge of collapsing  $R_c$  by<sup>22</sup>

$$\frac{R_j}{R_c} \approx 0.1. \quad (8.108)$$

The length of the jet,  $l_j$ , defined as the full travel path of the protruded liquid, is related to  $R_c$  by<sup>23</sup>

$$\frac{l_j}{R_c} \approx 3. \quad (8.109)$$

From these two ratios, the amount of liquid within the jet,  $V_j$ , can be estimated:<sup>24</sup>

$$V_j \approx 0.1 R_c^3. \quad (8.110)$$

---

<sup>21</sup>Postema M, van Wamel A, ten Cate FJ, de Jong N. High-speed photography during ultrasound illustrates potential therapeutic applications of microbubbles. *Med Phys* **2005** 32:3707–3711.

<sup>22</sup>Kodama T, Takayama K. Dynamic behavior of bubbles during extracorporeal shock-wave lithotripsy. *Ultrasound Med Biol* **1998** 24:723–738.

<sup>23</sup>Ohl CD, Ikink R. Shock-wave-induced jetting of micron-size bubbles. *Phys Rev Lett* **2003** 90:214 502.

<sup>24</sup>Ohl CD, Ory E. Aspherical bubble collapse — comparison with simulations. In Lauterborn W, Kurz T, eds., *Nonlinear Acoustics at the Turn of the Millennium*. New York: American Institute of Physics **2000** 393–396.

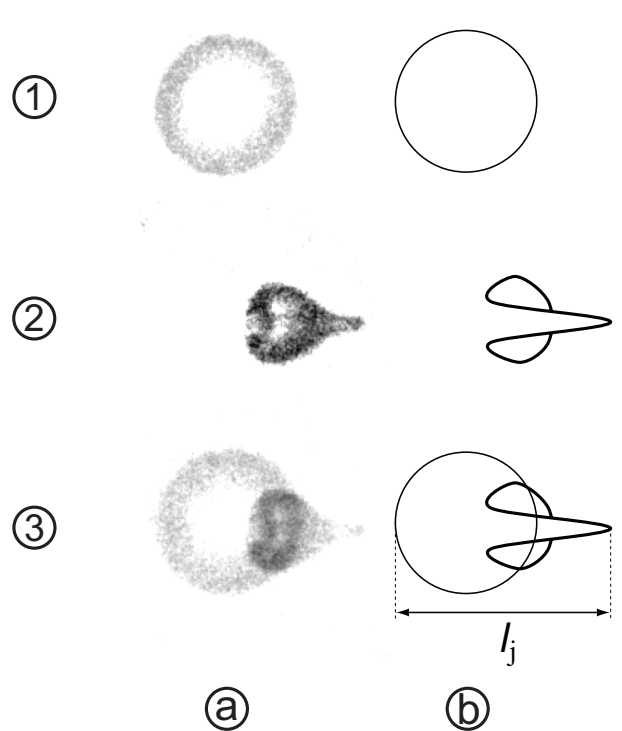


Figure 8.11: Two high-speed photographic frames (a1,2) and an overlaid image thereof (a3) of microjetting — a microbubble acting as a microsyringe — and a schematic representation of this phenomenon (b). On the verge of microjetting (1, thin line), the microbubble has a diameter of  $17 \mu\text{m}$ . During microjetting (2), liquid protrudes through the right side of the microbubble, over a length of  $l_j = 26 \mu\text{m}$ . The jet is represented by the bold curve. The time between the two frames is  $0.33 \mu\text{s}$ . Reprinted with permission from Postema M, van Wamel A, ten Cate FJ, de Jong N. High-speed photography during ultrasound illustrates potential therapeutic applications of microbubbles. *Med Phys* **2005** 32:3707–3711.

The impact of a jet on a surface generates a high pressure region. The pressure in this region has been referred to as water-hammer.<sup>25</sup> For a perfectly plastic impact, the water-hammer pressure of a cavitation jet is approxi-

<sup>25</sup>Cook SS. Erosion by water-hammer. *Proc Roy Soc London A* **1928** 119:481–488.

mately<sup>26</sup>

$$p_{\text{wh}} \approx \frac{1}{2} \rho c v_j, \quad (8.111)$$

where  $p_{\text{wh}}$  is the water-hammer pressure and  $v_j$  is the jet velocity.

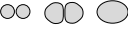
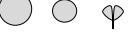
When administering microbubbles in the bloodstream, vessel walls are the boundaries to which ultrasound-induced jets are to be targeted. From high-speed optical observations of microjetting through ultrasound contrast agent microbubbles, it has been computed that the pressure at the tip of the jet is high enough to penetrate any human cell.<sup>27</sup> Therefore, it has been speculated whether liquid jets might act as microsyringes, delivering a drug to a region of interest.

Of influence on the occurrence of all the above-mentioned phenomena are (a) the ultrasonic parameters: transmit frequency, acoustic amplitude, pulse length, pulse repetition rate and transmit phase; (b) the ultrasound contrast agent composition: the composition of the shell, the bubble sizes, the size distribution and the gas; (c) the physical properties of the medium: viscosity, surface tension, saturation. Table 8.1 gives an overview of the nonlinear phenomena that have been observed with ultrasound contrast agents, the type of ultrasound contrast agent in which they have occurred, and the minimum acoustic regime required.

---

<sup>26</sup>de Haller P. Untersuchungen über die durch Kavitation hergerufenen Korrosionen. *Schweiz Bauzeit* **1933** 101:243–246.

<sup>27</sup>Postema M, van Wamel A, Lancée CT, de Jong N. Ultrasound-induced encapsulated microbubble phenomena. *Ultrasound Med Biol* **2004** 30:827–840.

Phenomenon	Schematic representation	Shell class <sup>1</sup>	Regime <sup>2</sup>
Translation		I, II, III, IV	L, M, H
Fragmentation		I, II	L, M, H
Coalescence		I, II	L, M, H
Jetting		I, II	H
Clustering		II, III	L, M, H
Cracking		II, III, IV	L, M, H

<sup>a</sup>Microbubble shell classes: (I) free or released gas; (II) thin shells < 10 nm; (III) thick shells < 500 nm; (IV) very thick shells > 500 nm.

<sup>b</sup>Acoustic regimes: low (L) for  $MI < 0.3$ ; medium (M) for  $0.3 < MI < 0.7$ ; high (H) for  $MI > 0.7$ .

Table 8.1: Nonlinear phenomena and their occurrence regimes.